International Journal of Environmental Impacts
https://www.acadlore.com/journals/IJEI

Heterogeneity and Landscape Resilience of Post-Eruption Vegetation at Mount Semeru-Indonesia Using Pixel-Based Unmanned Aerial Vehicles Analysis

Abdulkadir Rahardjanto[1,2], Ludwick Satria Romadoni[1], Husamah Husamah[1,2*], Tutut Indria Permana[1], Atok Miftachul Hudha[1,2], Ahmad Adnan Mohd Shukri[3], Listyo Yudha Irawan[4], Widodo Eko Prasetyo[5]

[1] Department of Biology Education, Faculty of Education, Science, and Humanities, Universitas Muhammadiyah Malang, 65144 Malang, Indonesia
[2] Magister of Biology Education, Postgraduate Program, Universitas Muhammadiyah Malang, 65144 Malang, Indonesia
[3] School of Educational Studies, Universiti Sains Malaysia, 11800 Penang, Malaysia
[4] Geography Department, Universitas Negeri Malang, 65145 Malang, Indonesia
[5] Department of Geomatics Engineering, Institut Teknologi Sepuluh Nopember, 60111 Surabaya, Indonesia

[*] Correspondence: Husamah Husamah (usya@umm.ac.id)

Received: 11-12-2025 **Revised:** 03-29-2026 **Accepted:** 05-08-2026

Citation: A. Rahardjanto, L. S. Romadoni, H. Husamah, T. I. Permana, A. M. Hudha, A. A. M. Shukri, L. Y. Irawan, and W. E. Prasetyo, "Heterogeneity and landscape resilience of post-eruption vegetation at Mount Semeru-Indonesia using pixel-based unmanned aerial vehicles analysis," *Int. J. Environ. Impacts.*, vol. 9, no. 4, pp. 897–907, 2026. https://doi.org/10.56578/ijei090405.

Abstract: The catastrophic 2021 eruption of Mount Semeru severely degraded local ecosystems, necessitating rapid pioneer vegetation establishment to restore landscape stability. While conventional satellite imagery often obscures critical micro-scale ecological interactions, ultra-high-resolution unmanned aerial vehicles (UAVs) provide an unprecedented tool for assessing post-disaster resilience. This study aimed to quantify the multitemporal recovery rate and model the micro-topographic constraints dictating the spatial heterogeneity of pioneer colonization. A 127.08-ha primary lahar corridor within Volcanic Hazard Zone III was mapped using UAVs (2.7 cm/pixel) over a three-year period (2022, 2023, 2025). Vegetation cover was extracted using the Excess Green (ExG) index and automated Otsu thresholding. The methodology was rigorously validated using 300 multitemporal ground-truth points, yielding an overall accuracy of 93.00%, an F1-score of 0.933, and a Cohen's Kappa coefficient of 0.860, confirming exceptional classification reliability. Post-classification spatial analysis revealed a net positive vegetation expansion rate of +1.88 ha/year, indicating a successful transition from initial colonization to ecological stabilization. However, recovery was profoundly heterogeneous, governed entirely by geomorphological constraints rather than uniform macro-climatic factors. Population-based zonal statistics identified significant ecological preferences for higher peripheral elevations (mean 3,081.0 m), gentler slopes acting as natural seed traps (45.5°), and Southwest-facing aspects that provide essential micro-climatic buffering against equatorial desiccation. These findings offer a strategic paradigm shift for environmental management, recommending that artificial restoration and erosion control interventions in active stratovolcanoes be precisely targeted at these highly resilient micro-topographical hotspots to accelerate the formation of a natural biological shield.

Keywords: Remote sensing; Spatial analysis; Semeru; Succession; Time-series analysis; Unmanned aerial vehicle; Vegetation recovery; Volcanic eruption

1 Introduction

The eruption of Mount Semeru on December 4, 2021, was a catastrophic natural disaster that triggered an acute ecological and humanitarian crisis in Lumajang Regency, East Java, Indonesia. The collapse of the lava dome generated massive pyroclastic and lahar flows that buried the Curah Kobokan plains, devastating the surrounding ecosystems. Initial post-eruption assessments identified over 2,331 ha of severely affected land, encompassing vital natural forests, agricultural fields, and community plantations [1]. The profound loss of vegetation cover not only decimated local biodiversity but also severely destabilized the geomorphology of the landscape. In such highly disturbed volcanic environments, the rapid re-establishment of vegetation a process known as primary succession is the most critical natural mechanism for restoring landscape stability, preventing catastrophic secondary erosion, and rebuilding essential ecosystem services [2, 3].

Research on post-eruption ecosystem recovery and landscape resilience in Indonesia has predominantly relied on satellite-based remote sensing. For instance, a seminal study successfully modeled the spatial resilience of the Mount Merapi ecosystem by analyzing land cover transitions from open volcanic deposits to vegetated land using multitemporal Landsat imagery [3]. A similar macro-scale approach was employed at Mount Unzen, Japan, utilizing a Landsat time-series to model landscape recovery rates [4]. While invaluable for assessing regional-scale recovery, these satellite-based studies possess significant methodological limitations. The relatively coarse spatial resolution of freely available satellite imagery e.g., 30 meters for Landsat often obscures critical micro-scale ecological interactions [5, 6]. Furthermore, researchers emphasize that resulting land cover classifications are often too general to detect species-level changes [7–10] and frequently fail to capture the influence of micro-topography on pioneer seed survivability [11–14]. Consequently, there is an urgent and widely recognized call for more detailed research utilizing remote sensing imagery with much higher spatial resolution [15–20].

The advancement of unmanned aerial vehicle (UAV) technology presents a transformative solution to this resolution gap, offering a highly precise tool for environmental management and disaster impact assessment. UAVs can flexibly acquire ultra-high spatial resolution imagery centimeter-level (<5 cm/pixel) below the cloud cover. In the Semeru context, preliminary studies have demonstrated the efficacy of UAVs for rapid geomorphological damage assessment immediately following the eruption [21–23]. Furthermore, the workflow for quantifying vegetation growth parameters from UAV time-series [22] data has been well-established in other disciplines, proving capable of constructing high-precision growth curves and extracting metrics like canopy area [24, 25]. Adapting this high-precision phenotyping methodology to an ecological succession context allows researchers to shift from landscape-level to plot-level analysis [26–31]. However, the application of ultra-high-resolution UAV time-series data to quantitatively model the spatial heterogeneity of early vegetation resilience and its micro-topographic constraints remains largely unexplored in tropical volcanic settings.

This study aims to fill this critical methodological and ecological gap by conducting a pixel-based landscape analysis of post-eruption vegetation resilience. A 127.08-ha Area of Interest (AOI) within the Volcanic Hazard Zone III (Kawasan Rawan Bencana/KRB III) was purposively selected, as it represents the most heavily impacted primary lahar corridor, serving as an ideal laboratory for observing the limits of ecological endurance. The specific objectives are to: (1) quantify the multi-temporal rate of vegetation recovery to evaluate overall landscape resilience; (2) map the spatial heterogeneity of recovery density; and (3) model the macro-topographic constraints (elevation, slope, and aspect) that dictate the spatial distribution of pioneer vegetation. By linking spatial recovery patterns with geomorphic controls, this research provides a vital scientific foundation for environmental management, enabling local authorities and conservation agencies to design targeted, evidence-based interventions for erosion control and ecological restoration in hazardous volcanic landscapes.

2 Methodology

2.1 Research Design and Study Area

This study employed a quantitative longitudinal design to model the spatial heterogeneity of early vegetation resilience following the Mount Semeru eruption. The research is administratively located in Pronojiwo District, Lumajang Regency, East Java, Indonesia. To ensure a robust landscape-scale analysis, a continuous wall-to-wall mapping approach was applied to a primary AOI covering 127.08 ha. This specific AOI size and location were purposively delineated because it encompasses the primary lahar corridor within Volcanic Hazard Zone III (KRB III) the area subjected to the most severe pyroclastic and debris flow impacts. Therefore, it serves as an ideal and representative spatial laboratory for evaluating the geomorphological constraints on pioneer vegetation establishment in highly disturbed environments (see Figure 1).

2.2 Data Acquisition and Acccuracy Assessment

Primary spatial data consisted of ultra-high-resolution optical imagery acquired using a rotary-wing UAV. To capture the critical phases of primary succession, data acquisition was strategically conducted during the dry seasons (to minimize cloud cover) at three distinct time points: June 2022, June 2023, and June 2025. This specific temporal spacing was designed to evaluate two distinct ecological phases: the initial one-year interval (2022–2023) captures the rapid, short-term colonization rate of pioneer species, while the subsequent two-year interval (2023–2025) evaluates the stabilization and survival capacity of this new growth against secondary geomorphological disturbances. The study area experiences a uniform tropical monsoonal climate; thus, macro-climatic factors (such as the >2000 mm/year regional rainfall) were treated as a constant baseline rather than variable drivers of spatial heterogeneity.

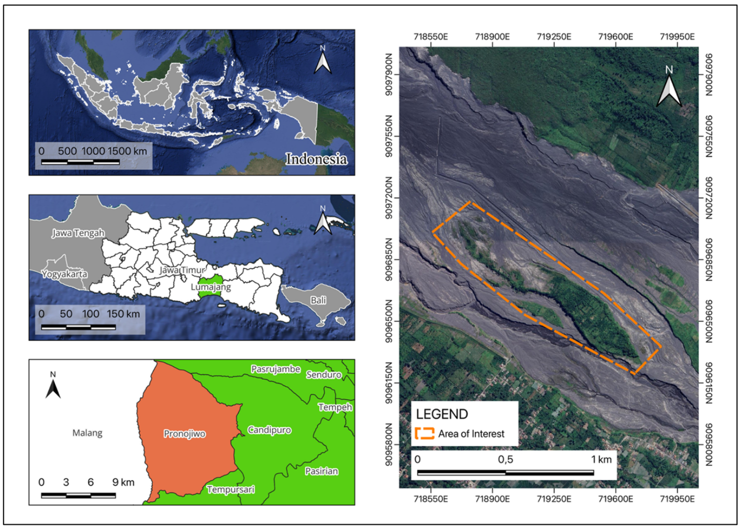

Figure 1. Research area map

All flight missions were executed at a consistent altitude of 110 meters Above Ground Level (AGL), ensuring an ultra-high spatial resolution of 2.7 cm/pixel. To guarantee multi-temporal comparability and spatial precision, a robust network of 12 Ground Control Points (GCPs) was established using Geodetic GPS. These GCPs were strategically distributed across the relatively stable margins of the AOI to avoid the highly dynamic and inaccessible lahar channels. Furthermore, an extensive set of 24 Independent Check Points (ICPs) was deployed per observation year to objectively validate the positional accuracy without influencing the photogrammetric model calibration.

Given the extreme and inaccessible nature of the post-eruption volcanic terrain, the multitemporal orthorectification process yielded exceptional and consistent spatial accuracy across all observation periods. To quantitatively evaluate the geometric reliability, the positional deviations between the orthomosaic coordinates (X_i, Y_i) and the reference GPS coordinates (X_{ref}, Y_{ref}) from the ICPs were calculated. The Root Mean Square Error (RMSE) for both X and Y axes, the combined horizontal error (RMSE_{xy}), and the Circular Error at 90% confidence (CE90) were determined using the following established photogrammetric equations:

$$\text{RMSE}_x = \sqrt{\frac{\sum_{i=1}^{n} (X_i - X_{ref})^2}{n}}$$

$$\text{RMSE}_y = \sqrt{\frac{\sum_{i=1}^{n} (Y_i - Y_{ref})^2}{n}}$$

$$\text{RMSE}_{xy} = \sqrt{\text{RMSE}_x^2 + \text{RMSE}_y^2}$$

$$\text{CE90} = 1.5175 \times \text{RMSE}_{xy}$$

As detailed in Table 1, the calculated CE90 values for 2022, 2023, and 2025 were consistently below the 1.5-meter threshold. According to the updated Indonesian Geospatial Information Agency standard (Peraturan Badan Informasi Geospasial No. 6 year 2018, amending Regulation No. 15 year 2014) for base map geometric accuracy, all multitemporal datasets strictly satisfy the highest spatial tolerance criteria (Class 1 Accuracy) for a 1:5,000 mapping scale.

Table 1. Accuracy evaluation based on 24 Independent Check Points (ICPs) per observation year

Observation Year	RMSE_x (m)	RMSE_y (m)	RMSE_{xy} (m)	CE90 (m)
2022	0.384	0.418	0.568	0.861
2023	0.389	0.382	0.545	0.828
2025	0.388	0.392	0.551	0.836

Note: RMSE, Root Mean Square Error; CE90, Circular Error at 90% confidence.

This rigorous geometric validation ensures that the subsequent multi-temporal landscape comparisons and zonal statistical analyses are positionally absolute and free from significant spatial misalignments. Finally, to ensure precise pixel-to-pixel temporal co-registration among the 2022, 2023, and 2025 orthomosaics, a manual image-to-image registration was performed utilizing permanent, undisturbed geomorphological features (e.g., massive bedrock boulders at the corridor margins) as fixed tie points.

2.3 Data Processing Procedure

The acquired UAV imagery was processed using a standard photogrammetric Structure-from-Motion (SfM) workflow to generate two primary geospatial datasets for each observation period: a Digital Elevation Model (DEM) and an RGB Orthomosaic.

To discriminate vegetation from bare volcanic substrates, the Excess Green (ExG) vegetation index was calculated using the formula $ExG = 2G - R - B$. The ExG index was explicitly selected over other visible-band indices (such as Visible Atmospherically Resistant Index (VARI) or Green Leaf Index (GLI)) due to its superior sensitivity in isolating early-stage photosynthetic pigments against the highly reflective, bright-gray background of fresh volcanic ash. Subsequently, a binary land cover classification (Vegetation vs. Non-Vegetation) was executed using the automated Otsu thresholding algorithm, which objectively determines the optimal separation threshold based on the image histogram.

To rigorously evaluate the reliability of the ExG Otsu thresholding algorithm across the highly heterogeneous post-eruption landscape, an accuracy assessment was conducted using 300 ground-truth validation points distributed across the 2022–2025 temporal datasets. Given the imbalanced nature of volcanic landscapes where bare lahar deposits typically dominate over pioneer vegetation relying solely on overall accuracy can be misleading. Therefore, this study incorporated advanced evaluation metrics, including the F1-score and Cohen's Kappa coefficient. The assessment yielded a robust overall accuracy of 93.00% and a high F1-score of 0.932 for vegetation detection. Crucially, the Cohen's Kappa coefficient of 0.860 confirmed an almost perfect agreement between the automated UAV classification and the actual ground conditions, validating the robustness of the methodology for monitoring micro-scale ecological succession.

2.4 Data Analysis Techniques

2.4.1 Landscape resilience and transition analysis

To quantify the vegetation recovery rate, a post-classification comparison was performed. The binary maps from 2022, 2023, and 2025 were spatially intersected to create a transition matrix. The resulting pixel trajectories were grouped into ecological resilience categories (e.g., Stable Vegetation, Persisting New Growth, Temporary Vegetation). The net change rate was calculated using the stock difference method to determine the overall landscape balance between colonization and degradation over the three-year period.

2.4.2 Geomorphological constraints and zonal statistics

To identify the micro-topographic factors dictating recovery patterns, a wall-to-wall zonal statistical analysis was conducted. Unlike sample-based approaches, this study analyzed the entire pixel population within the 127.08 ha landscape. The classified vegetation map was utilized as the zone definition layer (recovery vs. non-recovery zones) to extract descriptive statistics from three primary topographic variables derived from the UAV-DEM: (1) elevation (mean and standard deviation), (2) slope (mean and standard deviation), and (3) aspect. Furthermore, a spatial density analysis with discrete classification bounds was executed to pinpoint statistically significant agglomerations of high vegetation resilience.

3 Results

3.1 Landscape Resilience and Spatiotemporal Recovery Rates

The multitemporal pixel-based analysis of the 127.08 ha AOI revealed a highly dynamic, yet distinctly resilient, post-eruption landscape. The rigorous accuracy assessment (overall accuracy = 93.00%; Cohen's Kappa = 0.860) ensures that the detected land cover transitions represent genuine ecological succession rather than classification artifacts. Table 2 details the spatial extent of these transition categories over the three-year observation period.

Table 2. Landscape resilience dynamics and vegetation cover transition within the 127.08 ha Volcanic Hazard Zone (2022–2025)

Change Category	Ecological Interpretation	Area (ha)
Stable Non-Vegetation	Highly unstable substrate	106.89
Stable Vegetation	Surviving ecosystem core	8.93
Persisting New Growth since 2023	Established pioneer colonization	4.38
Recent New Growth in 2025	Late-stage pioneer colonization	3.12
Temporary Vegetation	Failed succession	1.46
Recovered Vegetation Lost Then Regrew	Resilient recolonization post-secondary disturbance	0.94
Vegetation Loss in 2025	Recent secondary disturbance	0.90
Persistent Vegetation Loss since 2023	Persistent ecological degradation	0.43
Total AOI		127.08

Note: AOI, Area of Interest.

To visually contextualize these ecological dynamics, Figure 2 illustrates the spatial distribution of the landscape resilience categories. The map clearly demonstrates that while the core lahar paths remain largely unstable, the peripheral zones exhibit significant recolonization capacity.

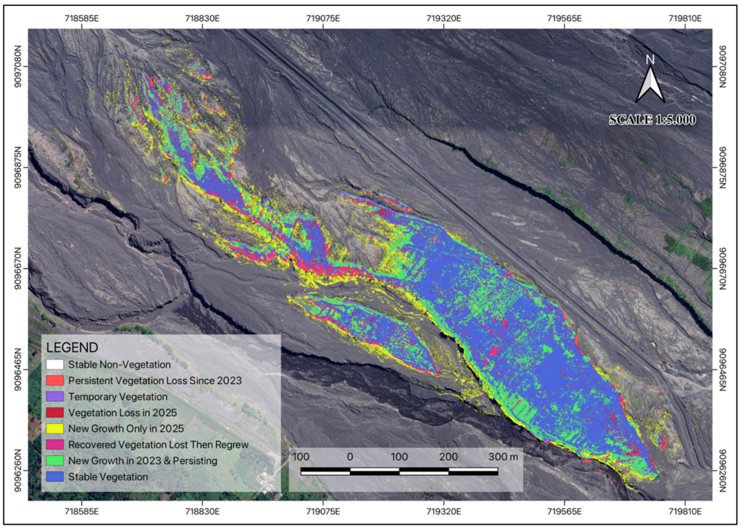

Figure 2. Spatial distribution of vegetation resilience and landscape transition categories within the 127.08 ha Volcanic Hazard Zone (2022–2025)

The landscape demonstrated a net positive vegetation recovery trajectory. Despite the persistent instability of the primary lahar beds (characterized by 106.89 ha of Stable Non-Vegetation), the ecosystem exhibited a steady colonization rate. The presence of 8.93 ha of 'Stable Vegetation' functions as critical undisturbed refugia, acting as primary seed sources for the surrounding degraded areas. Furthermore, the combined area of 'Persisting New Growth' (4.38 ha) and 'Recent New Growth' (3.12 ha) significantly outweighed the areas experiencing secondary vegetation loss. Quantitatively, the landscape achieved a net vegetation expansion rate of +1.88 ha per year. This positive net change during the crucial 2022–2025 window indicates that the early pioneer colonization phase has successfully transitioned into a stabilization phase, demonstrating robust intrinsic resilience against the harsh volcanic substrate.

3.2 Spatial Heterogeneity of Vegetation Density

While the overall net recovery is positive, the spatial distribution of this recolonization is profoundly heterogeneous. Figure 3 illustrates the vegetation recovery density, mapped using discrete classification bounds to highlight significant spatial agglomerations.

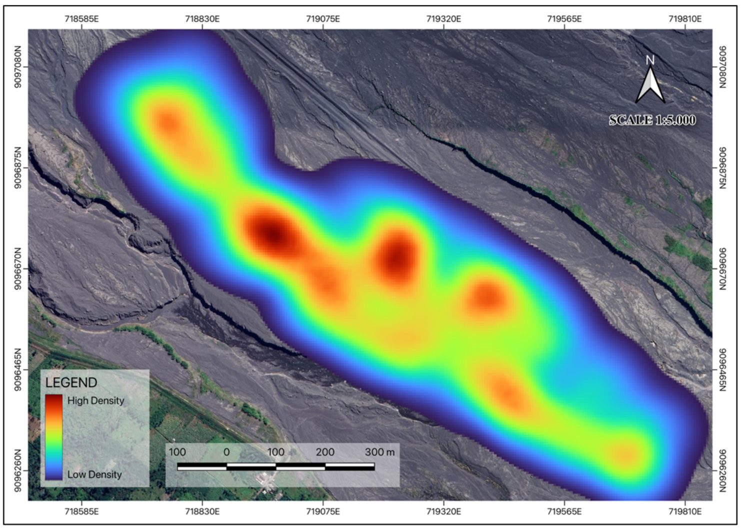

Figure 3. Spatial heterogeneity of pioneer vegetation recovery density

The density map reveals that pioneer vegetation does not colonize the volcanic deposits uniformly. Instead, recovery is highly clustered, forming distinct high-density "hotspots" predominantly located along the upper margins of the primary lahar corridor. The central, low-elevation paths of the corridor remain largely barren. This extreme spatial clustering strongly suggests that macro-climatic factors (such as regional rainfall) are not the primary drivers of succession in this localized 127.08 ha landscape. Rather, the survival and establishment of pioneer seeds are fundamentally dictated by micro-topographical constraints that govern physical stability and resource retention.

3.3 Macro-Topographical Constraints on Pioneer Colonization

To objectively determine the geomorphological rules governing these recovery hotspots, a wall-to-wall zonal statistical analysis was performed on the total pixel population of the UAV-DEM. By utilizing a complete spatial census rather than a sample-based approach, the extracted parameters represent true population parameters, eliminating sampling error. The analysis compared the topographic signatures of the vegetated 'recovery zone' against the barren 'non-recovery zone' (Table 3 and Figure 4).

Table 3 shows a distinct topographic dichotomy between recovery and non-recovery areas. Vegetation recovery is heavily concentrated at higher elevations (mean = 3,081.0 m, SD = 145.2 m) compared to the non-recovery areas (mean = 2,488.0 m, SD = 210.5 m). Ecologically, this suggests that the higher elevations within the KRB III zone likely function as lateral safe zones. While the lower elevations act as active depositional channels that are repeatedly scoured by secondary lahar flows during heavy monsoon rains, the higher peripheral elevations appear to remain physically stable enough to allow seedling root systems to anchor.

Table 3. Comparison of topographic statistics between recovery and non-recovery zones

Topographic Variable	Recovery Zone (Mean ± SD)	Non-Recovery Zone (Mean ± SD)	Difference
Elevation (m)	3,081.0 ± 145.2	2,488.0 ± 210.5	+593.0 m
Slope (°)	45.5 ± 6.3	50.2 ± 8.1	-4.7°

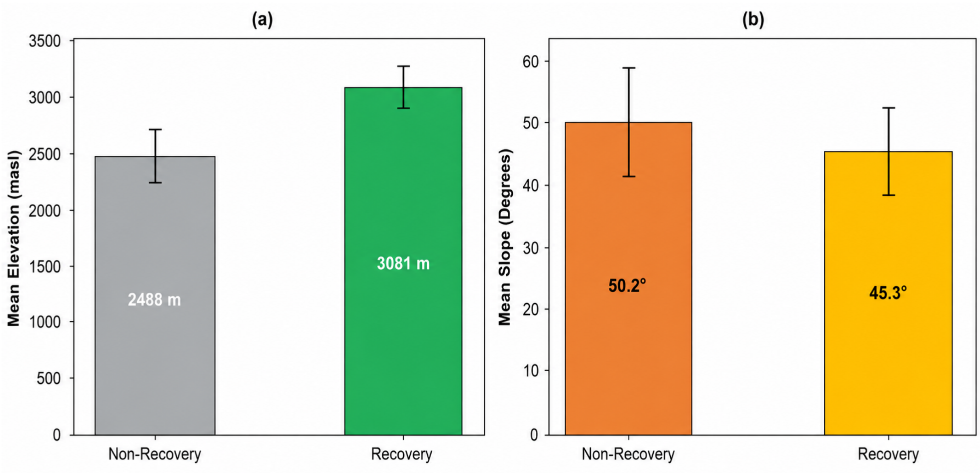

Figure 4. Topographic differences between recovery and non-recovery zones: (a) mean elevation; (b) mean slope

Similarly, slope acts as a critical geomorphological filter. Pioneer colonization shows a distinct spatial preference for relatively gentler inclines (mean = 45.5°) compared to the steeper barren zones (mean = 50.2°). In the context of highly porous and unconsolidated volcanic ash, steeper slopes are exceptionally vulnerable to rapid surface runoff and severe rill erosion. The gentler slopes in the recovery areas likely function as natural "seed traps", accumulating wind-blown pioneer seeds and retaining sufficient surface moisture to support germination before the substrate erodes. In Figure 4, the error bars represent the standard deviation, indicating the spatial dispersion of elevation and slope values within each zone.

The reliability of the vegetation–non-vegetation classification used to delineate these recovery patterns was further supported by the multi-temporal accuracy assessment presented in Table 4. Based on 300 ground-truth validation points, the ExG thresholding algorithm achieved an overall accuracy of 93.00%, with high user's accuracy for vegetation (96.00%) and non-vegetation (90.00%). The vegetation class also showed a strong F1-score of 0.933, while Cohen's Kappa reached 0.860, indicating substantial agreement between classified data and ground-truth observations. These results confirm that the mapped recovery zones provide a reliable basis for interpreting the geomorphological controls of vegetation recovery.

Table 4. Multi-temporal confusion matrix and rigorous accuracy assessment of the Excess Green (ExG) thresholding algorithm based on 300 ground-truth validation points (2022–2025)

Classified Data	Vegetation	Non-Vegetation	Total	User's Accuracy
Vegetation	144	6	150	96.00%
Non-vegetation	15	135	150	90.00%
Total	159	141	300	–
Producer's accuracy (Recall)	90.57%	95.74%	–	–
Overall accuracy	–	–	–	93.00%
F1-score (Vegetation)	–	–	–	0.933
Cohen's Kappa	–	–	–	0.860

Note: A dash (–) denotes no data.

The spatial heterogeneity of landscape resilience appears to be strongly influenced by slope aspect. As demonstrated in Figure 5, landscape resilience is overwhelmingly concentrated on Southwest-facing (SW) micro-sites. This directional preference is thought to be linked to the micro-climatic buffering capacity of the terrain. In tropical montane environments, Southwest-facing slopes may receive favorable photosynthetically active radiation during part of the day while being partially buffered from extreme direct insolation that can rapidly desiccate porous volcanic topsoil. By maintaining a slightly more stable soil moisture regime, these SW aspects may provide a more conducive micro-niche for early root development.

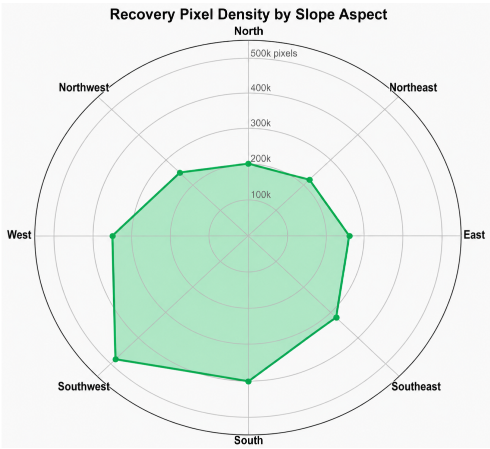

Figure 5. Spatial heterogeneity of landscape resilience based on slope aspect

3.4 Implications for Volcanic Environmental Management

The findings of this ultra-high-resolution spatial modeling offer actionable insights for environmental management and disaster mitigation. The identification of specific topographic niches (higher elevations, gentler slopes around 45.5°, and SW aspects) provides local forestry and conservation agencies with a precise spatial blueprint for artificial reforestation efforts. Rather than broadcasting seeds randomly across the unstable lahar corridor which often results in high mortality rates restoration interventions can be strategically targeted at these geomorphologically stable hotspots. Enhancing vegetation cover in these specific niches will likely accelerate the formation of a natural biological shield, significantly improve landscape stability and provide long term erosion control against secondary volcanic hazards. The methodological framework established here, utilizing UAV derived ExG indices coupled with population based zonal statistics, can serve as a highly transferable model for monitoring ecosystem resilience in other active stratovolcanoes across the tropics.

3.5 Limitations of the Study and Future Directions

While this study provides robust, high-resolution insights into early-stage landscape resilience, certain temporal limitations must be acknowledged. The three-year observation window (2022–2025) successfully captures the critical pioneer colonization and initial stabilization phases; however, it is insufficient to model the long-term climax community succession. Furthermore, the reliance on annual data acquisition necessitated by severe logistical and safety constraints in accessing the highly hazardous KRB III zone precludes the analysis of finer-scale seasonal vegetation dynamics. Future research should ideally incorporate higher frequency multitemporal monitoring (e.g., capturing wet versus dry season fluctuations) and extend the longitudinal baseline to fully comprehend the ultimate ecological trajectory of this recovering volcanic landscape.

4 Discussion

The data reveals a stark topographic dichotomy. Vegetation recovery is heavily concentrated at significantly higher elevations (mean = 3,081.0 m, SD = 145.2 m) compared to the non-recovery areas (mean = 2,488.0 m). Ecologically, these higher elevations within the KRB III zone function as lateral safe zones. While the lower elevations act as active depositional channels continuously scoured by secondary lahar flows during heavy monsoon rains, the higher peripheral elevations remain physically stable, allowing seedling root systems to anchor without being washed away.

Similarly, slope acts as a critical geomorphological filter. Pioneer colonization shows a distinct preference for relatively gentler inclines (mean = 45.5°) compared to the steeper barren zones (mean = 50.2°). In the context of highly porous and unconsolidated volcanic ash, steeper slopes are exceptionally vulnerable to rapid surface runoff and severe rill erosion. The gentler 45.5° slopes function as natural "seed traps", accumulating wind-blown pioneer seeds and retaining sufficient surface moisture to trigger germination before the substrate erodes.

Furthermore, the spatial heterogeneity is strongly influenced by slope aspect. As demonstrated in the radar chart (Figure 5), landscape resilience is overwhelmingly concentrated on SW micro-sites. This directional preference is intrinsically linked to the micro-climatic buffering capacity of the terrain. In tropical montane environments, Southwest-facing slopes typically receive optimal photosynthetically active radiation during the afternoon [32–34], while being partially sheltered from the extreme, direct midday equatorial insolation that rapidly desiccates the porous volcanic topsoil. By maintaining a slightly more stable soil moisture regime, these SW aspects provide the precise micro-niche required to sustain early root development in an otherwise hostile landscape [34, 35].

The findings of this ultra-high-resolution spatial modeling offer actionable insights for environmental management and disaster mitigation [32–36]. The identification of specific topographic niches (elevations ~3,081 m, slopes ~45.5°, and SW aspects) provides local forestry and conservation agencies with a precise spatial blueprint for artificial reforestation efforts. Rather than broadcasting seeds randomly across the unstable lahar corridor which often results in high mortality rates restoration interventions can be strategically targeted at these geomorphologically stable "hotspots".

Enhancing vegetation cover in these specific niches will rapidly accelerate the formation of a natural biological shield, significantly improve landscape stability and provide long-term erosion control against secondary volcanic hazards [37]. The methodological framework established here, utilizing UAV-derived ExG indices coupled with population-based zonal statistics, proves highly transferable for monitoring ecosystem resilience in other active stratovolcanoes across the tropics.

5 Conclusions

This study demonstrates the critical utility of ultra-high-resolution UAV imagery and population-based spatial analysis in decoding micro-scale ecological succession within highly disturbed volcanic environments. Over the 2022–2025 observation period, the primary lahar corridor of Mount Semeru exhibited robust intrinsic resilience, successfully transitioning from an initial pioneer colonization phase to a stable ecological expansion. However, the spatial trajectory of this recovery is profoundly heterogeneous and is not governed by uniform macro-climatic factors.

Instead, early landscape resilience is fundamentally dictated by macro-topographical constraints. Pioneer vegetation strongly favors specific geomorphological niches specifically higher peripheral elevations, gentler slopes acting as natural seed traps, and Southwest-facing aspects that provide crucial micro-climatic buffering. These stable micro-sites protect emerging root systems from secondary lahar scouring and extreme equatorial desiccation.

Consequently, these findings offer a strategic paradigm shift for post-eruption environmental management. Rather than employing uniform, landscape-wide reforestation strategies that often suffer high mortality rates in active depositional channels, conservation efforts should be precisely targeted at these identified topographic hotspots. Prioritizing artificial interventions within these geomorphologically stable niches will accelerate the formation of a natural biological shield, significantly enhancing long-term erosion control and landscape stability. Ultimately, this spatial methodology provides a highly transferable framework for assessing and managing ecological resilience in other active tropical stratovolcanoes.

Author Contributions

Conceptualization, A.R., L.S.R., and H.H.; methodology, H.H., T.I.P., A.M.H., A.A.M.S., L.Y.I., and W.E.P.; software, A.R., L.S.R., L.Y.I., and W.E.P.; validation, A.R., T.I.P., A.M.H., and A.A.M.S.; formal analysis, L.S.R., T.I.P., A.M.H., A.A.M.S., L.Y.I., and W.E.P.; data curation, L.S.R.; visualization, A.R. L.S.R., L.Y.I., and W.E.P.; supervision, H.H.; writing—original draft, L.S.R. and H.H.; writing—review & editing, A.R., H.H., T.I.P., A.M.H., and A.A.M.S. All authors have read and agreed to the published version of the manuscript.

Data Availability

The data used to support the findings of this study are available from the corresponding author upon request.

Acknowledgments

Thanks to the management of Bromo Tengger Semeru National Park for the permission granted for this research. The authors also thank the Department of Biology Education, Faculty of Teacher Training and Education, Universitas Muhammadiyah Malang for the supporting of the research and publication.

Conflicts of Interest

The authors declare no conflicts of interest.

References

[1] H. Hidayat, E. Azzahra, and F. Bioresita, "Analisa perubahan tutupan lahan akibat letusan Gunung Semeru Tahun 2021 dengan algoritma Random Forest (studi kasus: Kecamatan Pronojiwo, Kabupaten Lumajang)," *Geoid*, vol. 19, no. 2, pp. 236–245, 2024. https://doi.org/10.12962/geoid.v19i2.1179

[2] S. B. Kurniawan, A. Roziqin, A. Ahmad, M. M. Ahmad, B. D. Alfanda, D. S. A. Pambudi, N. S. M. Said, P. M. Abdul, and M. F. Imron, "Tackling marine pollution in the blue economy: Synergies between wastewater treatment technologies and governmental policies," *Mar. Pollut. Bull.*, vol. 222, 2026. https://doi.org/10.1016/j.marpolbul.2025.118627

[3] S. M. Efastri, R. W. Eriyanti, and D. Karmiyati, "Developing contextualized picture storybooks for disaster education: A Riau Malay approach to building resilience in young children," *Indian J. Inf. Sources Serv.*, vol. 16, no. 1, pp. 89–100, 2026. https://doi.org/10.51983/ijiss-2026.16.1.10

[4] H. Husamah, A. Rahardjanto, A. M. Hudha, L. S. Romadoni, A. Widyantopo, and R. Anggraeni, "UAV RGB excess green mapping of dense but low-diversity mangrove stands on Pagerungan Besar Island, Indonesia," *AACL Bioflux*, vol. 19, no. 2, pp. 468–481, 2026.

[5] F. A. C. Wibowo, A. D. Pramudya, T. Muttaqin, and M. N. A. Pangestu, "The importance of riparian vegetation in maintaining spring water quality in Yeh Penet Watershed, Bali, Indonesia," *Biodiversitas*, vol. 25, no. 5, pp. 2051–2062, 2024. https://doi.org/10.13057/biodiv/d250523

[6] R. Lai, T. Oguchi, and C. Zhong, "Evaluating spatiotemporal patterns of post-eruption vegetation recovery at Unzen Volcano, Japan, from Landsat Time Series," *Remote Sens.*, vol. 14, no. 21, 2022. https://doi.org/10.3390/rs14215419

[7] C. Bolyn, P. Lejeune, A. Michez, and N. Latte, "Mapping tree species proportions from satellite imagery using spectral–spatial deep learning," *Remote Sens. Environ.*, vol. 280, p. 113205, 2022. https://doi.org/10.1016/j.rse.2022.113205

[8] D. Rocchini, D. S. Boyd, J. B. Féret, G. M. Foody, K. S. He, A. Lausch, H. Nagendra, M. Wegmann, and N. Pettorelli, "Satellite remote sensing to monitor species diversity: Potential and pitfalls," *Remote Sens. Ecol. Conserv.*, vol. 2, no. 1, pp. 25–36, 2016. https://doi.org/10.1002/rse2.9

[9] A. Polyakova, S. Mukharamova, O. Yermolaev, and G. Shaykhutdinova, "Automated recognition of tree species composition of forest communities using Sentinel-2 satellite data," *Remote Sens.*, vol. 15, no. 2, p. 329, 2023. https://doi.org/10.3390/rs15020329

[10] G. Coldea, D. Gafta, L. Filipaş, and A. I. Stoica, "No decline in plant species diversity despite noticeable land use changes over 58 years (Carpathian Foothills, Romania)," *Earth Syst. Environ.*, vol. 10, pp. 4345–4361, 2026. https://doi.org/10.1007/s41748-025-00853-2

[11] P. M. Ramsay, G. E. Prado, L. Tumi, G. P. Vadillo, and M. L. Suni, "Topography, seed dispersal, and climate change reduce future habitat for an endangered tropical high-altitude plant," *Biol. Divers.*, vol. 2, no. 2-3, pp. 95–105, 2025. https://doi.org/10.1002/bod2.70007

[12] A. Taghavi-Bayat, M. Gerke, and B. Riedel, "Soil moisture retrieval at high spatial resolution over alpine ecosystems on Nagqu-Tibetan plateau: A comparative study on semiempirical and machine learning approaches," *Sci. Remote Sens.*, vol. 9, p. 100135, 2024. https://doi.org/10.1016/j.srs.2024.100135

[13] P. Karami, S. Tavakoli, and M. Esmaeili, "Fine-scale satellite-based monitoring of temperature and vegetation cover in microclimates, distribution ranges, and landscape connectivity for Neurergus kaiseri (Kaiser's mountain newt) during the breeding season," *Ecol. Indic.*, vol. 170, p. 113077, 2025. https://doi.org/10.1016/j.ecolind.2025.113077

[14] K. Chytrý, N. Helm, K. Hülber, D. Moser, J. Wessely, J. Hausharter, A. Kollert, A. Mayr, M. Rutzinger, M. Winkler, and et al., "Limited impact of microtopography on alpine plant distribution," *Ecography*, vol. 2024, no. 2, p. e06744, 2024. https://doi.org/10.1111/ecog.06744

[15] H. Fang, G. He, L. Huang, C. Zhao, J. Wang, Y. Han, Q. Gao, T. Zhang, and J. Meng, "Altered flow and sediment transport impacts on the ecosystems of Chinese major rivers: An urgent call for eco-fluvial dynamics," *River*, vol. 3, no. 4, pp. 341–361, 2024. https://doi.org/10.1002/rvr2.110

[16] J. Park, "Review on remote sensing data-based stream mapping algorithms," *For. Sci. Technol.*, vol. 9, no. 2, pp. 87–96, 2013. https://doi.org/10.1080/21580103.2013.801161

[17] E. Rahimi and C. Jung, "Evaluating the applicability of landsat 8 data for global time series analysis," *Front. Remote Sens.*, vol. 5, p. 1492534, 2024. https://doi.org/10.3389/frsen.2024.1492534

[18] G. Bakó, Z. Molnár, L. Bakk, F. Horváth, L. Fehér, Örs Ábrám, E. Morvai, C. Biro, G. Pápay, A. Fűrész, and et al., "Toward a high spatial resolution aerial monitoring network for nature conservation—How can remote sensing help protect natural area?" *Sustainability*, vol. 13, no. 16, p. 8807, 2021. https://doi.org/10.3390/su13168807

[19] R. G. Kerry, F. J. P. Montalbo, R. Das, S. Patra, G. P. Mahapatra, G. K. Maurya, V. Nayak, A. B. Jena, K. E. Ukhurebor, R. C. Jena, and et al., "An overview of remote monitoring methods in biodiversity conservation," *Environ. Sci. Pollut. Res. Int.*, vol. 29, no. 53, pp. 80 179–80 221, 2022. https://doi.org/10.1007/s11356-022-232 42-y

[20] M. Pleniou and N. Koutsias, "The role of spectral vs spatial resolution of satellite data on the accuracy of mapping unburned vegetation within fire scar perimeters," *Sci. Remote Sens.*, vol. 11, p. 100241, 2025. https://doi.org/10.1016/j.srs.2025.100241

[21] K. Keränen, A. Isoaho, A. Räsänen, J. Hjort, T. Kumpula, P. Korpelainen, and P. Rana, "Multi-resolution remote sensing for flark area detection in boreal aapa mires," *Int. J. Remote Sens.*, vol. 45, no. 13, pp. 4324–4343, 2024. https://doi.org/10.1080/01431161.2024.2359732

[22] X. Chen, Y. Liu, F. Li, X. Li, and X. Jia, "Remote sensing image recommendation based on spatial–temporal embedding topic model," *Comput. Geosci.*, vol. 157, p. 104935, 2021. https://doi.org/10.1016/j.cageo.2021.104 935

[23] M. A. Hamel and S. Andréfouët, "Using very high resolution remote sensing for the management of coral reef fisheries: Review and perspectives," *Mar. Pollut. Bull.*, vol. 60, no. 9, pp. 1397–1405, 2010. https: //doi.org/10.1016/j.marpolbul.2010.07.002

[24] Z. A. Pierrat, T. S. Magney, W. P. Richardson, B. R. K. Runkle, J. L. Diehl, X. Yang, W. Woodgate, W. K. Smith, M. R. Johnston, Y. R. S. Ginting, and et al., "Proximal remote sensing: An essential tool for bridging the gap between high-resolution ecosystem monitoring and global ecology," *New Phytol.*, vol. 246, no. 2, pp. 419–436, 2025. https://doi.org/10.1111/nph.20405

[25] F. A. Kurnianto, M. Naim, A. Susiati, and D. A. J. Susanti, "Insight into the 2021 Semeru volcano eruption from rapid monitoring of its pyroclastic deposits using Google Earth Engine and multi-sensor data," *Remote Sens. Appl. Soc. Environ.*, vol. 36, p. 101380, 2024. https://doi.org/10.1016/j.rsase.2024.101380

[26] S. Bachri, E. H. Sanjaya, S. Sendari, R. P. Shrestha, and L. Y. Irawan, "The development of disaster risk map for Semeru Volcano eruption 2021–2022, East Java, Indonesia," *Indones. J. Geogr.*, vol. 56, no. 3, pp. 446–455, 2024. https://doi.org/10.22146/ijg.89918

[27] L. S. Romadoni, H. Husamah, and B. Ganiyu, "Accuracy comparison of remote sensing methods (UAV, LiDAR, Radar) and field allometry in mangrove blue carbon quantification: A systematic literature review," *Green Trop. Lab. Sustain.*, vol. 2, no. 2, pp. 58–61, 2025. https://doi.org/10.22219/gtlabs.v2i2.43380

[28] S. Rasti, C. J. Bleakley, N. M. Holden, R. Whetton, D. Langton, and G. O'Hare, "A survey of high resolution image processing techniques for cereal crop growth monitoring," *Inf. Process. Agric.*, vol. 9, no. 2, pp. 300–315, 2022. https://doi.org/10.1016/j.inpa.2021.02.005

[29] O. Bongomin, J. Lamo, J. M. Guina, C. Okello, G. G. Ocen, M. Obura, S. Alibu, C. A. Owino, A. Akwero, and S. Ojok, "UAV image acquisition and processing for high-throughput phenotyping in agricultural research and breeding programs," *Plant Phenome J.*, vol. 7, no. 1, p. e20096, 2024. https://doi.org/10.1002/ppj2.20096

[30] R. Greco, E. Barca, P. Raumonen, M. Persia, and P. Tartarino, "Methodology for measuring dendrometric parameters in a mediterranean forest with UAVs flying inside forest," *Int. J. Appl. Earth Obs. Geoinf.*, vol. 122, p. 103426, 2023. https://doi.org/10.1016/j.jag.2023.103426

[31] N. Guimarães, L. Pádua, P. Marques, N. Silva, E. Peres, and J. J. Sousa, "Forestry remote sensing from unmanned aerial vehicles: A review focusing on the data, processing and potentialities," *Remote Sens.*, vol. 12, no. 6, p. 1046, 2020. https://doi.org/10.3390/rs12061046

[32] C. Zhang, J. Valente, L. Kooistra, L. Guo, and W. Wang, "Orchard management with small unmanned aerial vehicles: A survey of sensing and analysis approaches," *Precis. Agric.*, vol. 22, no. 6, pp. 2007–2052, 2021. https://doi.org/10.1007/s11119-021-09813-y

[33] U. G. Sefercik, I. Aydin, M. Nazar, C. Atalay, and T. Kavzoglu, "A novel NDSM fusion approach to improve UAV-Based LCC accuracy in sloping urban areas," *Eur. J. Remote Sens.*, vol. 58, no. 1, p. 2475171, 2025. https://doi.org/10.1080/22797254.2025.2475171

[34] R. Zarychta and A. Zarychta, "Application of geostatistical approach in generating DEM for relief studies using UAV in forest areas," *Geomorphology*, vol. 487, p. 109916, 2025. https://doi.org/10.1016/j.geomorph.2025.10 9916

[35] B. Gano, S. Bhadra, J. M. Vilbig, N. Ahmed, V. Sagan, and N. Shakoor, "Drone-based imaging sensors, techniques, and applications in plant phenotyping for crop breeding: A comprehensive review," *Plant Phenome J.*, vol. 7, no. 1, p. e20100, 2024. https://doi.org/10.1002/ppj2.20100

[36] C. Zhong, T. Oguchi, and R. Lai, "Effects of topography on vegetation recovery after shallow landslides in the Obara and Shobara districts, Japan," *Remote Sens.*, vol. 15, no. 16, p. 3994, 2023. https://doi.org/10.3390/rs15163994

[37] Y. Zhong, X. Hu, C. Luo, X. Wang, J. Zhao, and L. Zhang, "WHU-Hi: UAV-borne hyperspectral with high spatial resolution (H2) benchmark datasets and classifier for precise crop identification based on deep convolutional neural network with CRF," *Remote Sens. Environ.*, vol. 250, p. 112012, 2020. https://doi.org/10.1016/j.rse.2020.112012